Research Paper
Journal of Aerospace System Engineering
Vol.15, No.2, pp.26-35 (2021)
EISSN 2508-7150
http://dx.doi.org/10.20910/JASE.2021.15.2.26

Numerical Analysis of the Effect of Fuselage of Fan-in-body Aircraft on the Pusher Propeller

Jiwook Kang [1,†], Jisung Jang[1], Younghyun You[1], Youngo Hyun[1] and Jonghun Lee[1]
[1]Aerospace Technology Research Institute, Agency for Defense Development

Abstract

In this study, CFD analysis was conducted to compare the aerodynamic performance of the isolated propeller and pusher propeller, which is affected by the wake of wide fuselage. The moving reference frame (MRF) method was used for isolated propeller analysis, while the MRF and sliding mesh method were used sequentially for the pusher propeller to analyze the change in the aerodynamic characteristics based on the azimuth angle. Under the same torque condition, the thrust of the pusher propeller was greater than that of the isolated propeller. Thrust increment of the pusher propeller was mainly generated near the root of the blade where the fuselage wake was concentrated. The net efficiency of the pusher propeller was greater than or equal to that of the isolated propeller. Because of the flat fuselage shape, thrust and torque of the pusher propeller periodically changed with the rotation of the propeller.

Key Words: Compound Rotorcraft, Fan-in-body, CFD, Pusher propeller

1. Introduction

The traditional rotorcraft has wide military and civilian applications owing to its capability of vertical takeoff and landing. However, because of the rotor aerodynamic characteristics, the rotorcraft is limited in its maximum forward flight speed, and thus, the forward flight range is smaller than that of a fixed-wing aircraft. Active R&D has been conducted on the compound rotorcraft with an auxiliary lift or horizontal propulsion system to overcome the limitations of existing rotorcraft and enable high-speed forward flight [1]. Among these types of rotorcraft, the fan-in-body aircraft has a lifting fan in the fuselage to achieve lift using a fan-in-body during hovering and low-speed forward flight. In high-speed forward flight, the fan is covered, obtaining forward thrust with a horizontal propulsion system, which operates like a regular fixed-wing aircraft. F-35B of Lockheed Martin and Phantom Swift of Boeing are representative aircraft that employ the fan-in-body concept.

Most of the recently developed compound rotorcraft such as the X^3, S-97 Raider, and SB-1 Defiant use propellers to obtain additional forward thrust. Generally, it is known that the propeller performance varies depending on the mounting configuration. According to Fage [2], in the case of a pusher propeller with a propeller behind the fuselage, the fuselage drag increases and the overall propulsive efficiency is lower than that of the tractor propeller with a propeller in front of the fuselage.

Received: Dec. 17, 2020 Revised: Jan. 21, 2021 Accepted: Jan. 26, 2021
† Corresponding Author
Tel: +82-42-607-6106, E-mail: jwkangsheep@add.re.kr

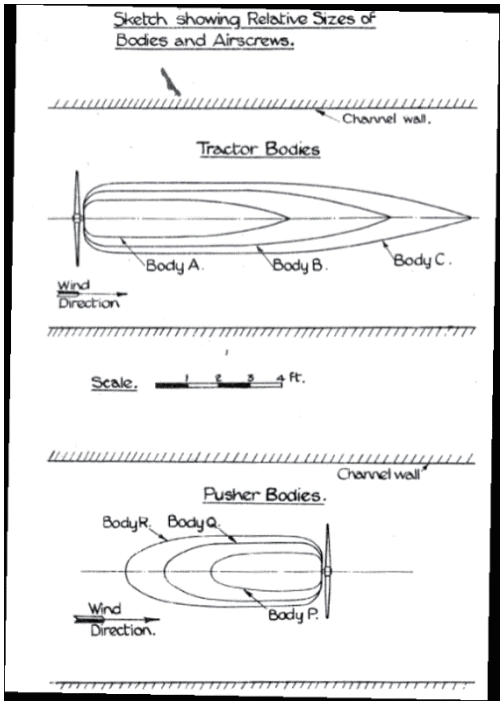

Fig. 1 Tractor and Pusher Configurations Comparison

In Fage's experiment, a fuselage shape with a blunt rear was used as shown in Figure 1, whereas Bateman's research using a streamlined fuselage shape showed that the pusher propeller was more efficient than the tractor propeller. According to Bateman's research with a streamlined fuselage as shown in Figure 2, both the tractor propeller and pusher propeller are less efficient than the isolated propeller, but the pusher propeller has a higher efficiency than the tractor propeller [3]. In McLemore's wind-tunnel test, unlike the findings of previous studies, the pusher propeller showed higher efficiency than other mounting configurations [4]. Moffitt performed CFD using three solvers and wind-tunnel tests for a fuselage suitable for high-speed rotorcraft, calculated the thrust and required power of the propeller according to the presence or absence of the fuselage, and performed cross-validation of the result. This analysis confirmed the result of improved propeller performance with the fuselage and explained the result with the concept of boundary layer ingestion [5]. Min et al. [6] obtained similar results to Moffitt's research in their analysis and experimental testing on the developed S-97 fuselage.

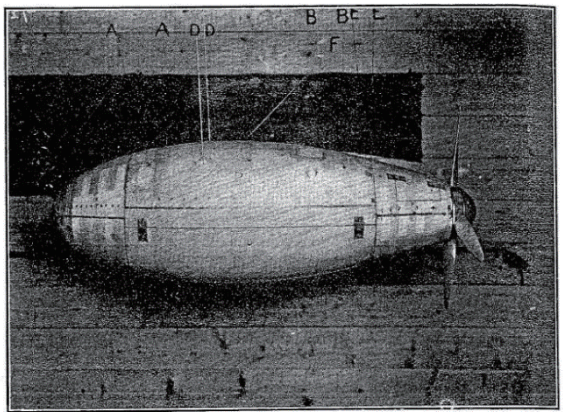

Fig. 2 Pusher Configuration tested by BARC[3]

Moffitt's work and most other related works used an axisymmetric fuselage geometry similar to a cylinder in the investigation of the fuselage–propeller relationship. However, in the case of fan-in-body aircraft, because the fan is located inside the fuselage, the length and width of the fuselage are larger than the height in most cases. Therefore, it is expected that wake patterns different from those of the axisymmetric fuselage used in previous studies will be observed, which is expected to have a different effect on the propeller.

In this study, thrust and torque of the pusher propeller affected by a wide fuselage are calculated, the calculation results are compared with those of an isolated propeller, and the impact of fuselage wake on the aerodynamic performance of the propeller is analyzed. To this end, first, the CFD result of a single propeller was compared with the wind-tunnel test result to verify the reliability of the CFD analysis. Then, to analyze the periodicity of the effect of non-axisymmetric fuselage wake according to the propeller rotation, the thrust and torque of the propeller were examined with changes in the propeller azimuth angle.

2. Analysis on aerodynamic performance of the propeller

2.1 Test of performance analysis method

STAR-CCM+ 14.02 commercial CFD software was used for CFD analysis of the propeller [7]. Before performing propeller analysis to investigate the fuselage wake effect, the CFD results were compared with Biermann's wind-tunnel test results to confirm the reliability of the analysis using the above software [8]. Biermann calculated the thrust coefficient, power coefficient, and efficiency according to the advance

ratio and blade pitch using a wind-tunnel test with a 10-foot-diameter 3-blade propeller 5868-9 with a Clark Y airfoil section. The geometry information of the propeller is illustrated in Figure 3. The geometric pitch indicated in Figure 3 is the case where the pitch angle of the r/R = 0.75 section is 15°. Here, b is the section chord length, D is the propeller diameter, r is the radius for each location, R is the propeller radius, h is the section thickness, and P is the geometric pitch. Here, the relationship between the geometric pitch P and blade pitch angle β is shown in Eq.1.

$$P = \pi D \tan\beta \quad (1)$$

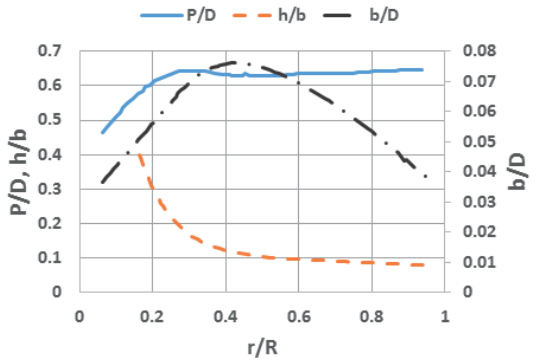

Fig. 3 5868-9 Blade Property

A 3D analysis model was developed using the propeller geometry information, as shown in Figure 4. As shown in Figure 5, the total analysis domain was created in the form of a sphere with a radius of 80 m. The domain for simulating the rotation of the propeller was composed of a cylinder with a height of 0.6 m and a radius of 2.2 m in the center of the sphere. In the experiment, the nacelle at the rear of the propeller and the spinner in the center of the propeller was present, but in the simulation for the test of the software, these two parts were not included. The increase in thrust by the spinner calculated in the experiment was only 2.5% at maximum, so it was determined that not including a spinner would not have a significant effect on the result.

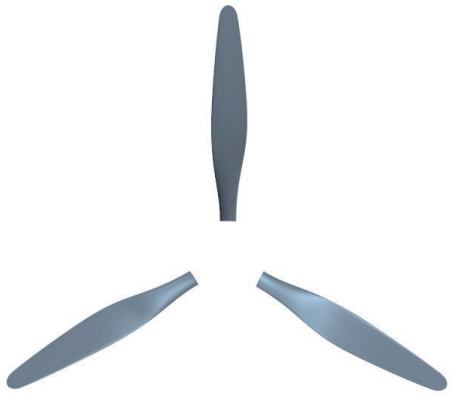

Fig. 4 3D model of the Propeller

The total number of meshes was about 28.4 million, of which about 2 million were in non-rotating domain and 26.4 million in rotating domain. For better depiction of the complex flow around the blade, meshes were composed of higher density around the blade. The mesh type used in the analysis is an unstructured polyhedral mesh provided by the software, which is based on tetrahedral mesh, was used. The first mesh size of the blade wall was set so that the blade surface y^+ satisfied $y^+ \cong 1$.

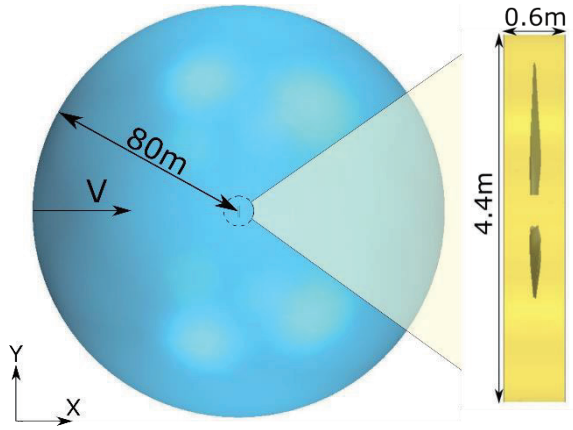

Fig. 5 Geometry of the Analysis Domain and the Propeller Domain

The 3D RANS (Reynolds Averaged Navier-Stokes) equation was used, and because the velocity of the blade tip is close to the Mach number 0.5, the solver also considered the compressible flow. The $k-\omega$ SST model was used as the turbulence model, and the segregated flow technique was used for the velocity–pressure relationship. For boundary conditions, the velocity inlet condition was applied to the entire boundary area.

For the analysis, moving reference frame (MRF) and sliding mesh (SM) methods were used for a propeller pitch angle of 15°. The MRF method was used for steady-state analysis, and the SM method was used for an unsteady state analysis through seven internal iterations at 2° intervals. The rotation speed was 1,000 rpm, and the forward speed was changed so that the

advance ratio matched with the experimental result, and the thrust coefficient C_T, the power coefficient C_P, and the efficiency η were calculated according to the forward speed. To reduce the instability at the initial stage of rotation, the rotation speed was increased linearly in the initial 400 iterations of the analysis. Each coefficient and efficiency were obtained from the equation below.

$$C_T = \frac{T}{\rho n^2 D^4} \tag{2}$$

$$C_P = \frac{P}{\rho n^3 D^5} \tag{3}$$

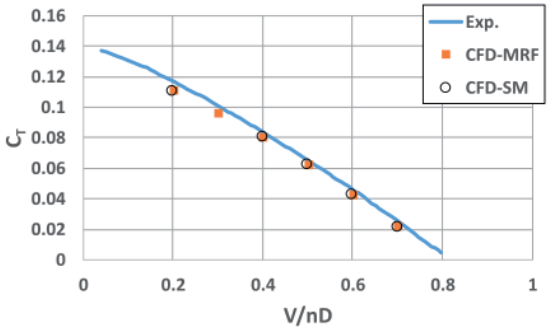

(a) Thrust Coefficient

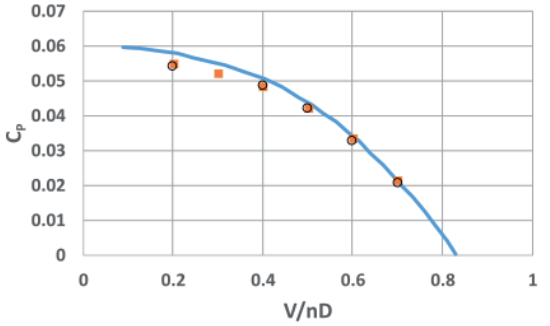

(b) Power Coefficient

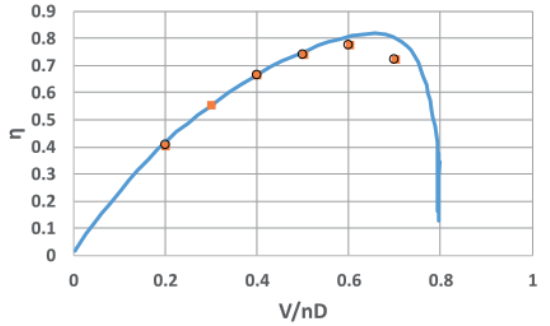

(c) Propeller Efficiency

Fig. 6 Comparison of CFD Results to Wind-Tunnel Test

$$\eta = \frac{VT}{P} = J\frac{C_T}{C_P} \tag{4}$$

where T is the propeller thrust, P is the propeller power, ρ is the air density, n is the number of rotations per second of the propeller, D is the propeller diameter, and J is the advance ratio, expressed as the ratio of the forward speed V and the rotation speed nD.

The comparison between the wind-tunnel test result and the CFD result is shown in Figure 6, and each coefficient according to the advance ratio is identical to the wind-tunnel test result in both the MRF and SM methods. For both MRF and SM methods, when J = 0.7, the efficiency value was different from the value of the wind-tunnel test, but the thrust coefficient and power coefficient were similar to the wind-tunnel test result, and thus this analysis method was determined to be reliable.

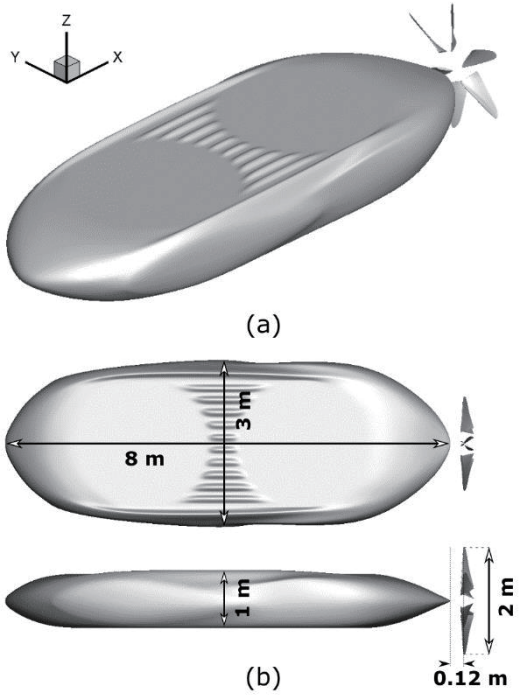

Fig. 7 Geometry of the Fuselage and Propeller; (a) in Isometric View (b) Top View and Side View

2.2 Fuselage-Propeller geometry and analysis method

To examine the effect of fuselage wake on the propeller, the isolated propeller and the pusher propeller mounted behind the fuselage were analyzed, respectively. The overall geometry of the fuselage used

in the pusher propeller analysis is shown in Figure 7(a). The length of the fuselage is 8 m, width at 3 m, and the height at 1 m, as shown in Figure 7(b). The propeller used in the analysis consists of six blades and the NACA23012 airfoil is applied. Its diameter is 2 m, and the chord length and twist angle according to the radius are shown in Figure 8. The distance between the propeller and fuselage is defined as the minimum distance between the rotating surface of the propeller and the end of the fuselage, and the value of 0.12 m was used in this analysis. The entire analysis domain is a sphere with a radius of 80 m as used for the software verification.

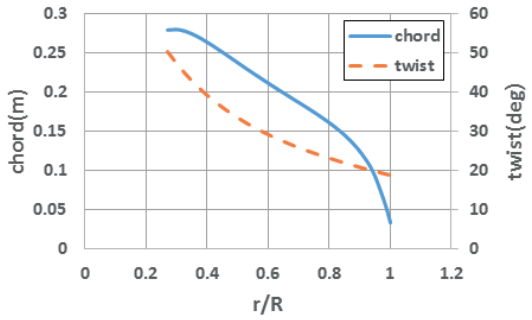

Fig. 6 Pusher Propeller Blade Property

24.4 million meshes were used across the total analysis domain, and the schematic of the mesh is illustrated in Figure 9. For better depiction of the propeller and wake, about 12 million meshes were used with denser mesh concentration around the propeller as shown in Figure 9. The size of the first mesh from the wall was set to satisfy $y^+ \cong 1$ around the blade surface.

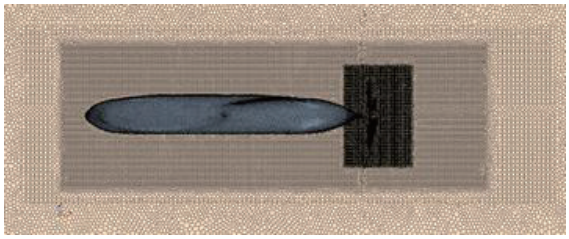

Fig. 7 Mesh around the Fuselage and the Propeller

The same turbulence model, velocity inlet condition, and velocity–pressure relationship that were used in the software verification at Section 2.1 were used in the analysis environment. The rotation speed of the propeller was fixed at 2,290 rpm. The analysis conditions for advance ratio and blade pitch angle are shown in Table 1. In Table 1, 'Isolated' indicates an isolated propeller, 'Pusher' indicates a pusher propeller, and 'Both' indicate both configurations. The advance ratio used for analysis changed from J =0.48 to J =1.44 with intervals of 0.24 at a pitch angle of 34°. In addition, to examine the effect of the pitch angle of the blade on the propeller efficiency at the same advance ratio, the analysis was performed at a pitch angle range from 29° to 39°.

For propeller analysis, the MRF and SM methods applied for software verification were used. Only the MRF method was used for the analysis of isolated propeller, and the MRF method and SM methods were used in sequence for the pusher propeller analysis. First, the MRF method was used in the analysis for fast convergence and then the SM method was used. Rotation at intervals of 1° and 10 times of internal iterations were applied. Because the propeller analysis is heavily influenced by fuselage wake, a shorter rotation interval and more internal iterations were used than those used for verification. For the aerodynamic result of CFD analysis, the average value for the last one rotation was used among the analysis results of total five rotations of the unsteady analysis. Because the rotation was applied after convergence with the MRF method, the CFD result was converged within three rotations under all analysis conditions.

Table 1 Analysis Conditions

Advance Ratio	Propeller Type	Pitch Angle(°)
0.24	Both	34
0.48	Both	34
0.72	Both	34
0.96	Both	34
1.20	Isolated	29, 32, 34, 36, 39
	Pusher	27, 29, 34, 39
1.44	Both	34

2.3 Fuselage wake and propeller efficiency

The propulsion by the propeller affected by the fuselage wake is commonly referred to as wake

ingestion or boundary layer ingestion(BLI) propulsion. According to the research of McLemore and Moffitt et al., the increase in the propeller efficiency with wake ingestion or boundary layer ingestion is caused by the inflow velocity faced by the propeller becoming smaller than the free stream speed because of fuselage [4,5]. Therefore, the definition of Eq. 4, which is mainly used for the propeller efficiency calculation, is not suitable in this case. To address this problem, the effective thrust $T_e = D - D_0$, which is obtained by subtracting the increment of the fuselage drag by the propeller from the increased propeller thrust, was used and the net efficiency η_p will be used, which was presented by McLemore as shown in Eq. 5, where D is the fuselage drag with a propeller, and D_0 is the fuselage drag without a propeller.

$$\eta_p = \frac{VT_e}{P} = \frac{V(T-(D-D_0))}{P} \tag{5}$$

2.4 Fuselage wake and non-axisymmetric effect

To examine the effect of fuselage on the flow field around the propeller, wake analysis was performed using the fuselage alone. Figure 10 shows the distribution of forward speed at the propeller rotation surface in case of J =1.2, and the distribution is normalized using the forward speed. Of the two concentric circles, the outer circle represents the boundary outside the propeller, and the inner circle represents the boundary within the propeller. As shown in Figure 10, the parts with the decrease in the speed by the fuselage show concentrated distribution along the center and Y axis according to the fuselage geometry.

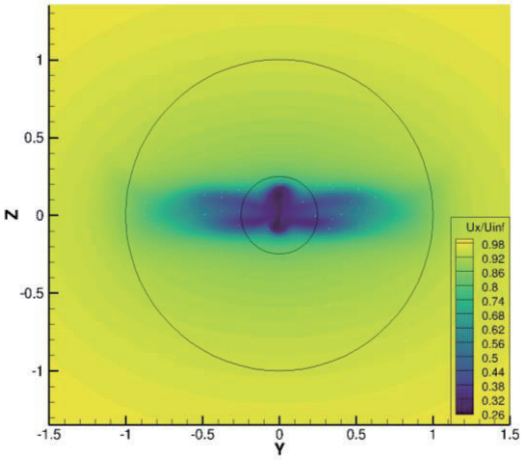

Fig. 8 Fuselage Wake Distribution

Thrust and torque were expected to vary according to the blade radial distance and azimuth angle by inflow distribution. To examine the thrust and torque, the section thrust coefficient and section torque coefficient of the blade were calculated. For the propeller radial distance r, the section thrust coefficient ΔC_T and the section torque coefficient ΔC_Q are calculated as shown in Equations 6 and 7.

$$\Delta C_T = \frac{\Delta T}{\rho n^2 D^4} \tag{6}$$

$$\Delta C_Q = \frac{\Delta Q}{\rho n^2 D^5} \tag{7}$$

Here, ρ is the air density, n is the propeller rotational speed, D is the propeller diameter, ΔT is the thrust at r, and ΔQ is the torque at r. ΔT and ΔQ were measured in the range of ±0.02 in the radial direction r.

3. CFD results

3.1 CFD result of a propeller

When the blade pitch angle is 34°, the CFD result of the propeller according to the advance ratio is shown in Figure 11(a) and Figure 11(b). Figure 11(a) shows the plot of torque coefficient versus the thrust coefficient. In this graph, the thrust-torque curve lies on the same straight line, indicating that the propeller performance did not change under the effect of fuselage wake. Figure 11(b) shows the curve of the propeller efficiency versus the thrust coefficient. According to the graph, when the thrust coefficient is the same, the pusher propeller showed approximately 10%-15% higher efficiency than the isolated propeller. In the case of net efficiency adjusted for fuselage drag, the pusher propeller efficiency was about 5% higher than that of the isolated propeller under the same thrust condition.

With J =1.2, the CFD results of the propeller according to the propeller pitch angle are shown in Figure 11(c) and Figure 11(d). In Figure 11(c), it can be seen that the torque of the pusher propeller is smaller than that of the isolated propeller under the same thrust condition. As for the propeller efficiency shown in Figure 11 (d), as in the case of the difference by the advance ratio, the pusher propeller showed higher efficiency than the isolated propeller under the same thrust condition, whereas net efficiency showed similar values across all values of the thrust. This shows that when fuselage wake affects the propeller, there is no performance

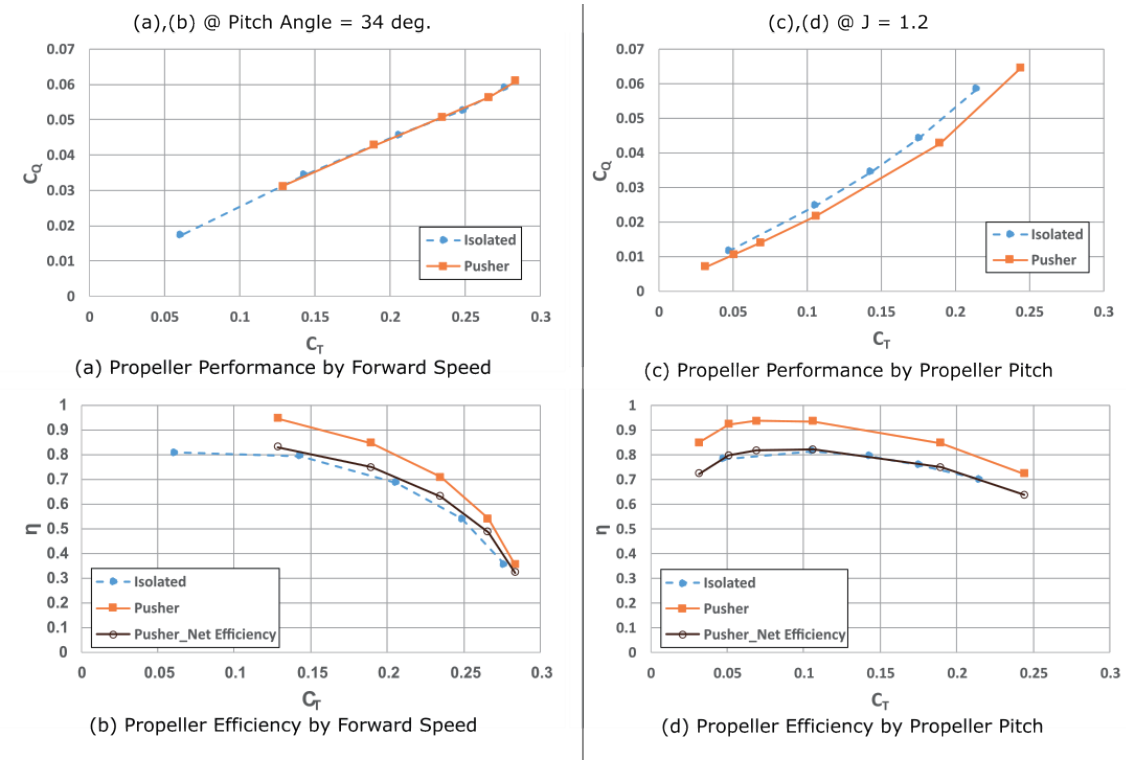

Fig. 9 Propeller Aerodynamic Characteristics

deterioration, or performance can be improved.

3.2 Analysis of the effect of fuselage wake on the propeller

3.2.1 Radial distribution of aerodynamic change

Figure 12 shows the section thrust coefficient and section torque coefficient of the isolated propeller and pusher propeller in the propeller radial direction. At J =1.2, cases of isolated propeller with pitch angle of 32° and pusher propeller with pitch angle of 29° were compared that satisfy similar thrust condition of $C_T \cong 0.106$. Here, the difference in the thrust coefficient between the two conditions was at 0.52%, indicating the same value. Because the inflow speed drop as a result of fuselage wake was concentrated in the center of the propeller, the section thrust of the pusher propeller was larger than that of the isolated propeller in the r/R<0.7 range.

In terms of section torque, in the range of r/R<0.5, the torque of the pusher propeller was slightly larger than that of the isolated propeller, but in the range of r/R>0.5, the section torque of the pusher propeller was smaller, indicating that the torque of the pusher propeller over the total range was 14.3% smaller. This can be considered that the higher efficiency was achieved by generating smaller torque under the same thrust condition. This result was consistent with the trend reported in Min's research [6].

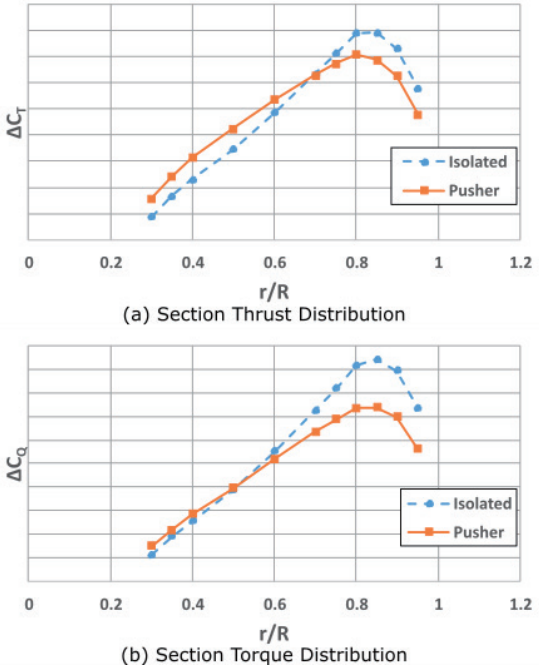

Fig. 10 Radial Thrust and Torque Distribution

3.2.2 Wake effect according to the blade azimuth angle

As shown in Figure 10, because the fuselage wake shows concentrated distribution in one direction, it was expected that the aerodynamic characteristics from the blade would change with the rotation of the propeller. To compare the blade location and the generated thrust, the azimuth angle φ was defined based on the +Z axis as shown in Figure 13.

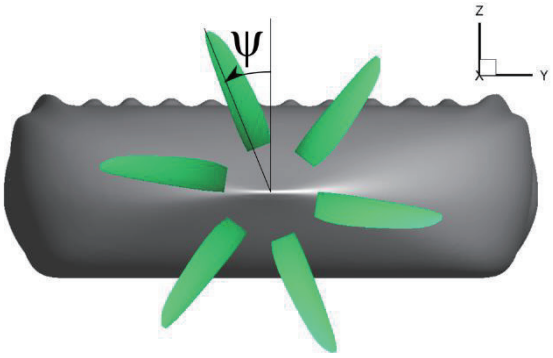

Fig. 11 Azimuth Angle Definition of Propeller Blade

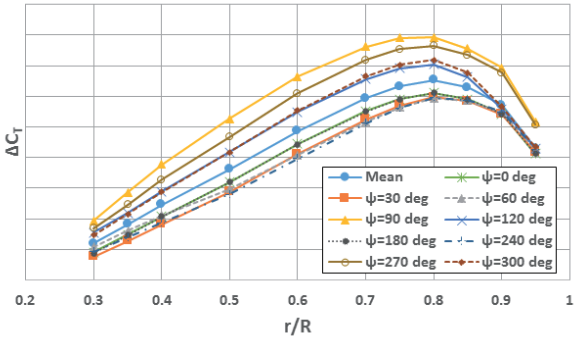

Fig. 12 Section Thrust Distribution

Figure 14 is a graph showing section thrust in the blade radial direction by blade azimuth angle when the propeller pitch angle is 34° and J =1.2. The highest thrust was observed at the azimuth angle of 90°, which was expected to be most affected by wake, while the thrust at 270°, which is in a symmetrical position from the angle of 90°, was smaller than that at 90°. This difference was attributed to a difference in flow velocity experienced by the blades occurring at each position as the vertical velocity component of the wake due to the fuselage rear geometry was added to the rotation velocity at blade azimuth angles of 90° and 270°.

Figure 15 shows the distribution of the vertical component of the fuselage wake according to the blade azimuth angle. Here, the vertical component was normalized with the propeller rotation velocity $V_\theta = r\omega$, and a value averaged in the range of r/R ±0.02 and azimuth angle ±5° was used. According to the azimuth angle, the wake vertical component showed a maximum difference of 7.36% at r/R=0.75 and a maximum difference of 13.03% at r/R=0.4.

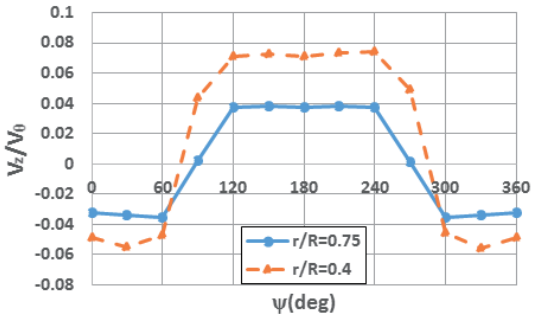

Fig. 13 Fuselage Vertical Wake Distribution

In the case of the azimuth angle of 60° and its symmetrical position at angle 240°, the same thrust was obtained in the r/R>0.6 region, but larger thrust was obtained at 60° in the r/R<0.6 region. However, the thrust was smaller than the average value for both azimuth angles. At azimuth angles of 120° and 300°, thrust larger than the average was obtained, and because these two angles were symmetrical positions, thrust showed a similar trend in all radial range. A larger thrust was generated on the side where the blade leaves the wake influence than on the side where the blade enters wake influence.

Figure 16 shows the section thrust coefficient distribution by the azimuth angle at r/R=0.75 and r/R=0.4 when propeller pitch angle is 34° and advance ratio is 1.2. The thrust coefficient used is not an average value, but a value calculated according to the blade azimuth angle during the last single rotation of the analysis. To compare the thrust at the blade symmetrical positions, one rotation was divided into the first half and the second half. The solid line represents the data in the azimuth angle range 1°~180°, and the dotted line represents the in the azimuth angle range 181°~360°. The most pronounced difference between the two data sets is in the range of 60°-120° and the symmetrical position, 240°-300°. In the case of r/R=0.75, the thrust increase due to wake effect occurred in the first half of the rotation, with the maximum value also occurring at

95°. In the second half of the rotation, the maximum value occurred at 99°, the actual azimuth angle of 279°. The difference in section thrust at the azimuth angle of 95° was 2.05%.

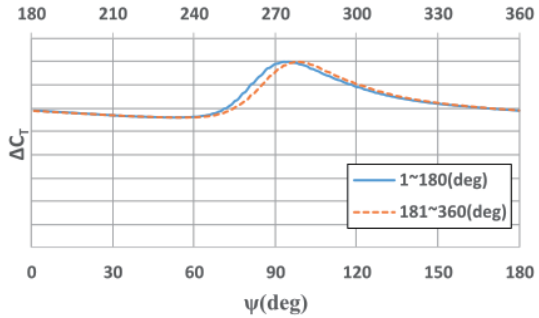

(a) Pitch = 34deg, J=1.2, r/R=0.75

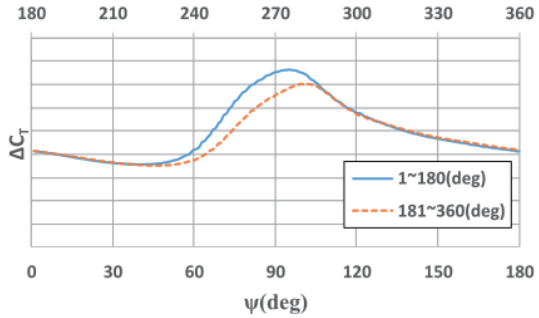

(b) Pitch = 34deg, J=1.2, r/R=0.4

Fig. 14 Section Thrust Distribution

As shown in Figure 16(b), the difference was more pronounced in the case of r/R=0.4 than r/R=0.75. The angle at which the maximum value occurred in the first half of the rotation was the same at 95°. However, in the second half of the rotation, the angle was 101° with the actual azimuth angle at 281°, indicating the occurrence of the maximum thrust at a larger angle later in the rotation. The difference in thrust at the azimuth angle of 95° was 8.18%, which was more than four times larger than the difference with r/R=0.75. As shown in Figure 16, this is thought to be due to the vertical component of the fuselage wake.

4. Conclusion

To investigate the effect of wide fuselage on the pusher propeller, aerodynamic characteristics were examined using a CFD program verified on the effectiveness and accuracy. The following results were obtained by observing the wake of the fuselage through CFD analysis of the flow field around the propeller.

(1) Under the condition of the same advance ratio and propeller pitch angle, the thrust, torque, and efficiency of the pusher propeller were larger than those of the isolated propeller.

(2) The net efficiency, adjusting for the increase in fuselage drag by the propeller, was larger or the same as that of the isolated propeller.

(3) The thrust of pusher propeller was larger than that of the isolated propeller in r/R<0.5 range where the fuselage wake effect was large, and the opposite applied in r/R>0.5 range. In addition, under the same thrust condition, the torque of the pusher propeller is small, increasing the efficiency.

(4) The extent of the influence of the fuselage wake varied according to the blade azimuth angle, and the generated thrust varies accordingly. The maximum thrust occurred around 90° and 270°, which are most affected by fuselage wake, and the minimum thrust occurred around 0° and 180°, which are the least affected by the wake.

In comprehensive consideration of the above results, we can see that the efficiency of the propeller in the fuselage wake is larger than that of the isolated propeller. Here, to further enhance the increment in efficiency, a fuselage shape design that minimizes the increase in fuselage drag will be required. In addition, because thrust in the radial direction has been showing different values from the conventional propeller, propeller design, considering the effect of fuselage wake will be required, unlike the existing propeller design method.

References

[1] J. G. Leishman, *Principle of Helicopter Aerodynamics*, 2nd Ed., Cambridge University Press, Cambridge, UK, pp. 47-49, 2006.

[2] A. Fage, C. N. H. Lock, R. G. Howard, and H. Bateman, "Experiments with a family of a airscrews including the effect of tractor and pusher bodies. Part 1. Experiments with a family of airscrews of a small body," *British Aeronautical Research Committee, Reports and Memorandum #829*, 1922.

[3] H. Bateman, F. C. Johansen, "Pressure and Force Measurement on Airscrew-body Combinations," *British Aeronautical Research Committee, Reports and Memorandum #1380*, 1930.

[4] H. C. McLemore, "Wind-Tunnel Tests of a 1/20-Scale Airship Model With Stern Propellers", *NASA Technical Note D-1026*, 1962

[5] B. Moffitt, P. Bowles, J. Joo, B. Y. Min, and B. Wake, "Analysis and Testing of Boundary-Layer-Ingesting Pusher Propeller for High Speed Rotorcraft," *AHS international 73rd Annual Forum & Technology Display*, Fort Worth, TX, USA, pp. 649-661, May 2017.

[6] B. Y. Min, B, Moffitt, P. O. Bowles, B. E. Wake, P. F. Lorber, "Analysis and Experimental Testing of S-97 RAIDERTM Propeller", AHS Specialists' *Conference on Aeromechanics Design for Transformative Vertical Flight*, San Francisco, CA, USA, pp. 757-767, Jan 2018.

[7] Siemens Product Lifecycle Management Software, "Simcenter STAR-CCM+ Release Notes: Version 2019.1.1," 2019.

[8] D. Biermann and E. P. Hartman, "Tests of two Full-scale Propellers With Different Pitch Distributions, at Blade Angles up to 60°," *Report No. 658, Technical Note NACA-TR-658*, pp. 1-4, 1938.